SANDIA REPORT

SAND2014-15497
Unlimited Release
Printed July 2014

Technique for the Estimation of Surface Temperatures from Embedded Temperature Sensing for Rapid, High Energy Surface Deposition

Tyson R. Watkins, P. Randall Schunk, and Scott A. Roberts

Prepared by
Sandia National Laboratories
Albuquerque, New Mexico 87185 and Livermore, California 94550

Sandia National Laboratories is a multi-program laboratory managed and operated by Sandia Corporation, a wholly owned subsidiary of Lockheed Martin Corporation, for the U.S. Department of Energy's National Nuclear Security Administration under contract DE-AC04-94AL85000.

Approved for public release; further dissemination unlimited.

Sandia National Laboratories

Issued by Sandia National Laboratories, operated for the United States Department of Energy by Sandia Corporation.

NOTICE: This report was prepared as an account of work sponsored by an agency of the United States Government. Neither the United States Government, nor any agency thereof, nor any of their employees, nor any of their contractors, subcontractors, or their employees, make any warranty, express or implied, or assume any legal liability or responsibility for the accuracy, completeness, or usefulness of any information, apparatus, product, or process disclosed, or represent that its use would not infringe privately owned rights. Reference herein to any specific commercial product, process, or service by trade name, trademark, manufacturer, or otherwise, does not necessarily constitute or imply its endorsement, recommendation, or favoring by the United States Government, any agency thereof, or any of their contractors or subcontractors. The views and opinions expressed herein do not necessarily state or reflect those of the United States Government, any agency thereof, or any of their contractors.

Printed in the United States of America. This report has been reproduced directly from the best available copy.

Available to DOE and DOE contractors from
U.S. Department of Energy
Office of Scientific and Technical Information
P.O. Box 62
Oak Ridge, TN 37831

Telephone: (865) 576-8401
Facsimile: (865) 576-5728
E-Mail: reports@adonis.osti.gov
Online ordering: http://www.osti.gov/bridge

Available to the public from
U.S. Department of Commerce
National Technical Information Service
5285 Port Royal Rd
Springfield, VA 22161

Telephone: (800) 553-6847
Facsimile: (703) 605-6900
E-Mail: orders@ntis.fedworld.gov
Online ordering: http://www.ntis.gov/help/ordermethods.asp?loc=7-4-0#online

SAND2014-15497
Unlimited Release
Printed July 2014

Technique for the Estimation of Surface Temperatures from Embedded Temperature Sensing for Rapid, High Energy Surface Deposition

Tyson R. Watkins and P. Randall Schunk
Nanoscale and Reactive Processes Department

Scott A. Roberts*
Fluid Sciences and Engineering Department

*Sandia National Laboratories
P.O. Box 5800
Albuquerque, NM 87185-0836
sarober@sandia.gov

Abstract

Temperature histories on the surface of a body that has been subjected to a rapid, high-energy surface deposition process can be difficult to determine, especially if it is impossible to directly observe the surface or attach a temperature sensor to it. In this report, we explore two methods for estimating the temperature history of the surface through the use of a sensor embedded within the body very near to the surface. First, the maximum sensor temperature is directly correlated with the peak surface temperature. However, it is observed that the sensor data is both delayed in time and greatly attenuated in magnitude, making this approach unfeasible. Secondly, we propose an algorithm that involves fitting the solution to a one-dimensional instantaneous energy solution problem to both the sensor data and to the results of a one-dimensional CVFEM code. This algorithm is shown to be able to estimate the surface temperature $\pm \sim 20°C$.

Acknowledgments

The authors gratefully acknowledge funding from the United States Office of Naval Research.

Contents

1 Introduction **9**

2 A model of the temperature history of an embedded probe **11**

2.1 Physical setup 11

2.2 Forward computational model 11

2.3 Embedded sensor sensitivity study 14

3 A robust temperature estimation algorithm using embedded sensor data **17**

3.1 Temperature estimation algorithm 17

3.2 Temperature estimation results 19

4 Conclusions **23**

List of Figures

2.1 Idealized tempreature profile for a single point on the surface due to the energy deposition. The location of T_s in time may be shifted to account for the fact that the energy deposition is moving across the surface of the bar. 12

2.2 Temperature distribution as the heat flux moves across top surface of the cube. 13

2.3 Heat flux condition at a particular z-location on the surface. 13

2.4 Temperature histories on the x symmetry plane, midway along the cube side. 15

3.1 Data from the forward simulation and estimated surface temperatures from the proposed algorithm including Gaussian noise up levels of a standard deviation of $5°C$. Data was taken from a sensor embedded at 1 mm depth. 19

3.2 Temperature profiles representing the bounding conditions. 20

3.3 Estimated bounds on surface temperatures for a sensor depth of 1 mm with Gaussian noise of $5°C$. 21

List of Tables

2.1 Peak temperatures at the surface and probe locations for each case in the sensitivity study of §2.3. 15

Chapter 1

Introduction

Temperature histories on the surface of a body are useful in many design efforts. However, in many situations, it is difficult to directly measure the heated surface of a solid. This may be because the geometry makes the heated surface inaccessible, or it may not be possible to directly attach a sensor on the surface. Even if conditions allow placement of a sensor directly on the surface, it is often difficult to achieve a high level of accuracy from these devices.

One possible solution is to embed a sensor in the solid itself. An embedded sensor could circumvent many of the issues identified with direct surface measurements. Ideally, one would embed such a sensor as close to the surface as possible in order to obtain the strongest signal. However, in materials with high thermal conductivities, such as metals, the temperature signal can be strongly attenuated, reducing the sensitivity of the technique. Nonetheless, these techniques have been used in applications such as grinding [4, 9, 13–15], where both thermocouples and optical fibers were used. Models have also been created to understand the behavior of these sensors [11, 12].

In order to obtain an estimate of the surface temperature from an embedded temperature sensor, an inverse heat conduction problem must be solved. In general, this inverse problem can be significantly more difficult than solving a direct heat conduction problem [1]. Inherent challenges in solving this inverse problem, especially for rapid heating processes, has been theoretically studied in great detail by Lambrakos and coworkers [5–7], who found the problem to be intractable for very rapid processes into diffusive materials such as metals. However, it might be possible to improve the accuracy of surface temperature estimations if some characteristics of the surface flux are known.

In the case of rapid, high energy surface deposition, the temperature field attenuates very quickly as the heat diffuses into the body. The temperatures very close to the surface can be orders of magnitude lower than those on the surface. In the inverse sense, the sensitivity of surface temperatures to peak temperatures within the body is very high, making the scheme sensitive to measurement errors. This requires that a robust method be created in order to minimize this sensitivity to measurement error from the embedded sensor.

With this work, we propose an inverse modeling technique for deducing the surface temperature history of a body that relies on some basic knowledge of the heat source and utilizes basic one-dimensional models of rapid heat deposition processes. A forward model

is used to provide computer experimental data to test this new technique (§2). This report is organized as follows: First, the physical system of interest is described in §2.1. A forward computational heat transfer model is presented in §2.2. In §2.3, the forward computational model was used to run different simulation cases to explore the sensitivity of the change in surface temperature to the maximum temperature of the transient response at a prescribed depth. This study draws conclusions on the requirements of an embedded sensor. Using the results of §2.3, a new inverse-model technique is proposed in §3, and this technique is tested in §3.2. Finally, in §4, we draw conclusion on the applicability of this method and propose future work to further test these ideas.

Chapter 2

A model of the temperature history of an embedded probe

2.1 Physical setup

The physical system explored in this study is an infinitely-long copper bar (z-direction), 60 mm wide (x-direction), and 30 mm thick (y-direction). A rapid, transient energy deposition process occurs on the top $y = 0$ surface of the bar. It affects a 30 mm wide strip, centered at $x = 0$, and runs down the z axis in the $+z$ direction. This energy deposition process moves with a constant velocity. The entire bar is insulated so that no heat exits the bar.

The properties of this energy deposition process were chosen to produce an idealized temperature profile on the surface, which is shown in Figure 2.1. This temperature profile is characterized by two distinct peaks. The highest temperature in the profile is denoted in Figure 2.1 as T_p, and we will refer to it as the primary surface temperature peak. The earlier, lower peak, T_s will be referred to as the secondary peak. After the passage of the energy deposition, which ends at the time where T_p occurs, t_p, the exponential decay in temperature is due to the heat diffusing into the bar. No further energy is injected into the system after t_p.

2.2 Forward computational model

In order to model the temperature throughout the bar described in §2.1, a computational heat transfer model was developed. This model solves the transient energy diffusion equation

$$\rho C_p \frac{\partial T}{\partial t} = k \nabla^2 T, \tag{2.1}$$

where ρ is the density, C_p is the heat capacity, T is the temperature, and k is the thermal conductivity. The thermophysical properties of the copper bar were held constant throughout the simulation. The values used were $\rho = 8933\,{}^{kg}/_{\mathrm{m}^3}$, $k = 401\,{}^{W}/_{\mathrm{m{\cdot}K}}$, and $C_p = 385\,{}^{J}/_{\mathrm{kg{\cdot}K}}$.

The interest in this model is to determine the temperature profile at some sensor location

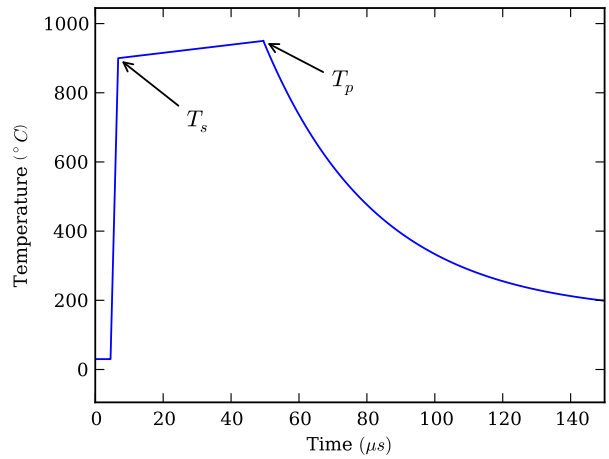

Figure 2.1: Idealized tempreature profile for a single point on the surface due to the energy deposition. The location of T_s in time may be shifted to account for the fact that the energy deposition is moving across the surface of the bar.

embedded closely (within 1 mm) beneath the surface. Because of these length scales of interest and for computational expediency, the entire length of the bar was not modeled. A sensitivity study of the geometry showed that accurate answers were obtained with a bar length of only 30 mm. Additionally, because the physical system (geometry and boundary conditions) are symmetric along the $x = 0$ plane, the geometry was modeled with symmetry boundary conditions along the $x = 0$ plane. The resulting geometry is a 30 mm cube, shown in Figure 2.2.

To achieve the desired surface temperature profile, the rapid, high energy deposition was modeled as a surface heat flux. This heat flux is applied to half of the top surface of the cube, making a 30 by 15 mm strip. The onset of heat flux starts at $z = 0\,\text{mm}$ and moves with a velocity $V_z = 2000\,{}^{m}/_{\text{s}}$. The flux profile has a limited duration and a unique shape which is large in magnitude during the initial contact and quickly decays to a lower flux level. The flux is parameterized as a piecewise function taking the form,

$$q(t,z) = \begin{cases} 0 & \text{for } t < \tau_z \\ A & \text{for } \tau_z \leq t < \tau_z + 0.05\Delta\tau \\ (A-D)e^{-B(t-\tau_z)} + D & \text{for } \tau_z + 0.05\Delta\tau \leq t \leq \tau_z + \Delta\tau \\ 0 & \text{for } t > \tau_z + \Delta\tau \end{cases}, \tag{2.2}$$

where A is the primary flux level (${}^{W}/_{\text{m}^2}$), D the secondary flux level (${}^{W}/_{\text{m}^2}$), and B is the flux decay (s^{-1}). τ_z represents the time in seconds associated with the onset of the heat flux boundary condition at a z-location and can be determined from the velocity and z-position by $\tau_z = z/V_z$. $\Delta\tau$ is the flux passage time and its value is determined by $\Delta\tau = 45\text{mm}/V_z$. At a given z-location in time on the surface of the block, the applied heat flux takes on a profile depicted in Figure 2.3. All other surfaces have adiabatic boundary conditions.

Figure 2.2 shows the temperature distribution for a sample simulation nearly halfway

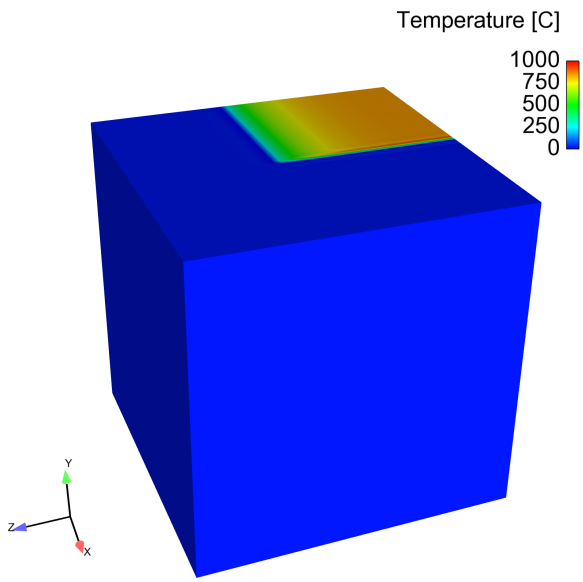

Figure 2.2: Temperature distribution as the heat flux moves across top surface of the cube.

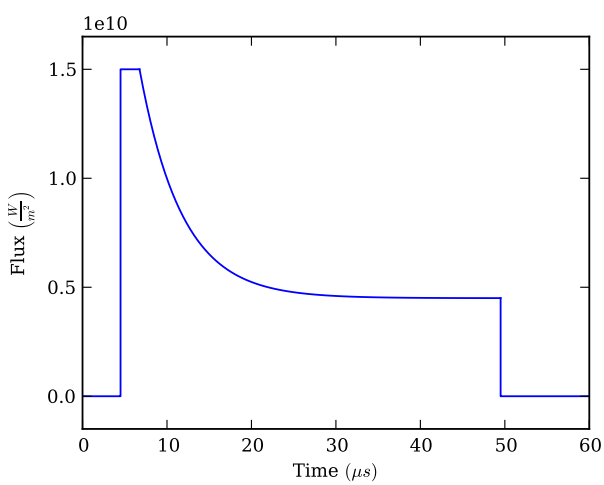

Figure 2.3: Heat flux condition at a particular z-location on the surface.

through the energy deposition process. The orange region represents the part of the surface where the energy has been deposited, causing the temperature to rise. The temperatures achieved in Figure 2.2 are nearly identical to the idealized temperature profile of Figure 2.1.

A hexahedral mesh of the geometry was created using Cubit [2], with mesh density highly biased towards the top surface and near the center of the geometry, in order to accurately capture the temperatures near the sensor. This model was implemented in the Galerkin-Finite Element Model code Sierra/Aria [10]. The temperature field was represented by tri-linear (Q1) elements, and a first-order time integration scheme was used, with adaptive time step adjustment.

A mesh and time refinement study were done to minimize errors due to spatial and temporal discretization. The spatial domain along the depth of the bar was continually refined until the deviation in the primary peak temperature on the surface was less than $0.1°C$. An adaptive time step scheme was used and the Predictor-Corrector tolerance was refined until the deviations in the peak temperature value were less than $0.1°C$.

The purpose of this model is to calculate the temperature distribution throughout the entire bar. The simulation output is probed along the centerline of the deposition ($x = 0$) in the center of the z computational domain. We are interested in an embedded probe that is placed either 0.5 mm or 1.0 mm from the heated surface. The temperature profiles at both of these locations are extracted and used in §2.3 to study the sensitivity of an embedded probe to changes in the surface temperature.

2.3 Embedded sensor sensitivity study

To explore the effects of surface temperatures on the temperature profiles at a given probe depth, a series of cases were organized. Initially, a baseline case was run in order to plan how the subsequent cases would deviate from this norm. The resulting surface temperature profile for this baseline case is shown in Figure 2.4a. The surface temperature history shows two distinct peaks: the secondary lower peak T_s and the primary higher peak T_p. These temperatures are shown as Case 1 in Table 2.1, and qualitatively correspond with the desired behavior shown in Figure 2.1.

Temperature measurements are taken at sensor locations at two desired depths, 0.5 mm and 1.0 mm. The behavior at the 1.0 mm sensor depth is shown in Figure 2.4b. Whereas the surface temperature exhibits two distinct peaks, the probe temperature shows a single maximum. This maximum temperature, denoted by $T_{max}^{0.5}$ for the 0.5 mm depth and $T_{max}^{1.0}$for the 1.0 mm depth, is used to quantify the temperature field at the sensor location, as shown in Table 2.1. For this baseline case, Figure 2.4 and Table 2.1 show that $T_{max}^{1.0}$is attenuated in magnitude by approximately 20 times compared to T_s and T_p. The time at $T_{max}^{1.0}$is also delayed by two orders of magnitude. This preliminary data suggests that directly using $T_{max}^{1.0}$to deduce the surface temperature may be problematic.

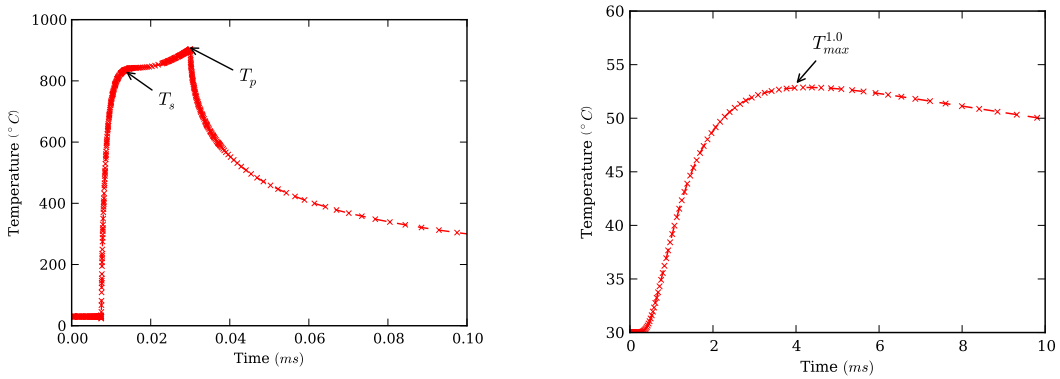

(a) Temperature profile on the surface.

(b) Temperature profile at a 1.0 mm depth.

Figure 2.4: Temperature histories on the x symmetry plane, midway along the cube side.

Case	T_s ($^\circ C$)	ΔT_s ($^\circ C$)	T_p ($^\circ C$)	ΔT_p ($^\circ C$)	δ ($^\circ C$)	$T^{0.5}_{max}$ ($^\circ C$)	$\Delta T^{0.5}_{max}$ ($^\circ C$)	$T^{1.0}_{max}$ ($^\circ C$)	$\Delta T^{1.0}_{max}$ ($^\circ C$)
1	842.28	-	904.23	-	61.95	75.74	-	52.87	-
2	862.97	20.69	904.69	0.46	41.72	76.30	0.55	53.15	0.28
3	809.50	-32.78	904.10	-0.13	94.60	75.04	-0.70	52.53	-0.35
4	840.83	-1.45	928.02	23.79	87.19	76.55	0.81	53.28	0.41
5	862.90	20.62	929.39	25.16	66.49	76.97	1.23	53.49	0.62
6	821.44	-20.84	924.40	20.17	102.96	75.98	0.23	52.99	0.12
7	842.27	-0.01	884.40	-19.83	42.13	75.16	-0.58	52.58	-0.29
8	855.76	13.48	884.57	-19.66	28.81	75.51	-0.23	52.76	-0.11
9	818.58	-23.70	883.06	-21.17	64.48	74.54	-1.21	52.26	-0.61

Table 2.1: Peak temperatures at the surface and probe locations for each case in the sensitivity study of §2.3.

The cases displayed in Table 2.1 were constructed to study the sensitivity of the probe temperature, T_{max}, to changes in the characteristic peaks of the surface temperature. To distinguish the effects of changes from either peak, they were varied separate from each other. Cases were defined as the combinations of separately raising and lowering the peaks by approximately $20°C$ from the baseline, resulting in nine different cases including the baseline. This allowed an observation of how the temperature response at the sensor locations changed with respect to the known surface temperature change.

The results of the simulations of each of these cases is found in Table 2.1, where the surface and sensor temperature are tabulated. Additionally, the difference between the two surface peak temperatures, or spread, $\delta = T_p - T_s$, is an important parameter in quantifying the nature of the surface temperature. ΔT_s and ΔT_p represent a deviation of the peak temperatures from the baseline case. Similarly, $\Delta T_{max}^{0.5}$ and $\Delta T_{max}^{1.0}$ correspond to the deviations from the maximum values of the baseline. These values were used to compute the signal sensitivity defined as the ratio of the change in the probe temperature to the change in secondary peak temperature, $S = \Delta T_{max}/\Delta T_s$.

Case 2 can be taken as a representative case for analysis. For case 2, the probe sensitivity to surface temperature, S, at the 0.5 mm and 1.0 mm locations are 2.7% and 1.3% respectively, which means that a very small change in T_{max} corresponds to a large change T_p. This shows that an embedded sensor, even one as close to the surface as 0.5 mm, is largely insensitive to changes in the surface temperature.

Initially, we desired to use the embedded sensor maximum temperature as a direct correlation to the peak surface temperature. The results from this sensitivity study give insight to the instrumentation that would be required to do this. To resolve $20°C$ on the surface, the sensor would have to be accurate to less than $1°C$. Even if a sensor could meet the speed and accuracy requirements, the sensitivities are such that inherent noise in the sensor signal would cause erroneous temperature estimations. This leads to the conclusion that a more robust estimation technique is required in order to resolve the surface temperatures to reasonable accuracy with the addition of noise in the sensor signal.

Chapter 3

A robust temperature estimation algorithm using embedded sensor data

In this chapter, we hope to improve on the naïve methodology of §2.3, where we attempted to use the maximum sensor temperature to directly deduce surface temperatures. In §3.1 we propose a new algorithm based on simple one-dimensional energy deposition models to regress the temperature sensor data. The algorithm is tested in §3.2.

3.1 Temperature estimation algorithm

In this section, we propose a new algorithm to use the temperature history taken from the embedded sensor and, in combination with simple one-dimensional energy deposition models, estimate the corresponding peak temperature on the surface. The first step of this algorithm is to extract the full temperature history ($T(t)$) from the sensor. For the purposes of this document, the forward simulations of §2.2 will be used as "computer experiments" to generate the sensor temperature history. These computer experiments are also useful as we also directly know the surface temperature from them, and algorithm can be tested by comparing against the computer experiments. These computer experiments from the forward model will be referred to as the "data" throughout the remainder of this chapter. In an actual deployment of this algorithm, the experimental sensor data would be used.

As shown by Figure 2.4, the time scale associated with the sensor location is two orders of magnitude greater than the flux passage time. At these slower time scales seen at the sensor location, the surface flux closely resembles a uniform, instantaneous pulse along the entire surface. Making this assumption suggests that the temperature response in the bar appears one-dimensional. This suggests that the solution to a one-dimensional energy deposition problem can be used to approximate the temperature throughout the bar. This problem was solved by [8], with an analytic form

$$T(y,t) = \frac{E}{\sqrt{\rho c_p k \pi (t-\gamma)}} e^{\left(\frac{-y^2}{4\alpha(t-\gamma)}\right)}, \tag{3.1}$$

where E is the total energy deposition per unit area (J/m^2), ρ is density (kg/m^3), c_p is specific heat (J/kgK), α is thermal diffusivity (m^2/s), k is thermal conductivity (W/mK), t is time, γ is

a time offset, and y is the depth (m). This analytic solution is used to fit unknowns E and γ to the computer experiment data. The time offset γ is added to the equation to allow the curve to be shifted either forward or backward in time, enabling it to capture the transient nature of the energy deposition process.

The temperature data at the sensor location is then fit to (3.1) using a Fortran code which implemented a non-linear Newton curve fit routine. Prior to the curve fit, random Gaussian noise of varying levels is added to the data to simulate the noise expected in the sensor signal. This fit yields regressed values for the total energy deposition E_{exp} and time offset γ_{exp}. The time offset γ_{exp} was found to be very sensitive to the addition of noise to the data and was discarded after the curve fit.

Because (3.1) is the solution for an instantaneous energy deposition, the initial surface temperature is ill-defined ($T(0,\gamma) = \infty$). Therefore, (3.1) is not directly suitable for determining the surface temperature. However, because the energy deposition process still closely resembles a one-dimensional process, a hybrid model was developed. This model uses a one-dimensional control-volume finite element method (CVFEM) code to model the temperature throughout the bar, subject to a surface heat flux. The parameterized heat flux (2.2) was modified slightly. The secondary flux level was set to a fraction of the primary flux level $D = \chi A$. This new parameter χ is what governs the spread δ between peaks and was set to the value corresponding to the baseline case $\chi = 0.27273$. The resulting modified boundary condition takes the form,

$$q(t,z) = \begin{cases} 0 & \text{if } t < \tau_z \\ A & \text{if } \tau_z \leq t < \tau_z + 0.05\Delta\tau \\ A\left((1-\chi)e^{-B(t-\tau_z)} + \chi\right) & \text{if } \tau_z + 0.05\Delta\tau \leq t \leq \tau_z + \Delta\tau \\ 0 & \text{if } t > \tau_z + \Delta\tau \end{cases}. \tag{3.2}$$

The CVFEM code is run and data extracted at the same depth as the experimental data. The CVFEM data is then curve fit using the same procedure described previously, which yields the total energy deposition for the simulation E_{sim}.

The CVFEM code runs inside of an optimization routine used to ensure $E_{sim} = E_{exp}$. This is accomplished by adjusting the heat flux level A of the CVFEM code based on the difference between E_{sim} and E_{exp}. With each new value of A, the CVFEM code is re-run, and this procedure is repeated until the difference of E_{sim} and E_{exp} is less than 10^{-6}. Using the final solution of the CVFEM simulation, the temperature history at the surface ($T(0,t)$) is extracted and, in this case, compared to the forward model data.

To summarize, the proposed procedure for this surface temperature estimation technique can be captured by the following algorithm:

1: Acquire temperature history from embedded sensor
2: Curve fit experimental sensor data to get total energy deposition level, E_{exp}
3: **while** $|E_{exp} - E_{sim}| > 10^{-6}$ **do**
4: Run the CVFEM code and extract simulation temperature history for sensor
5: Curve fit simulation sensor data to get total energy deposition level, E_{sim}

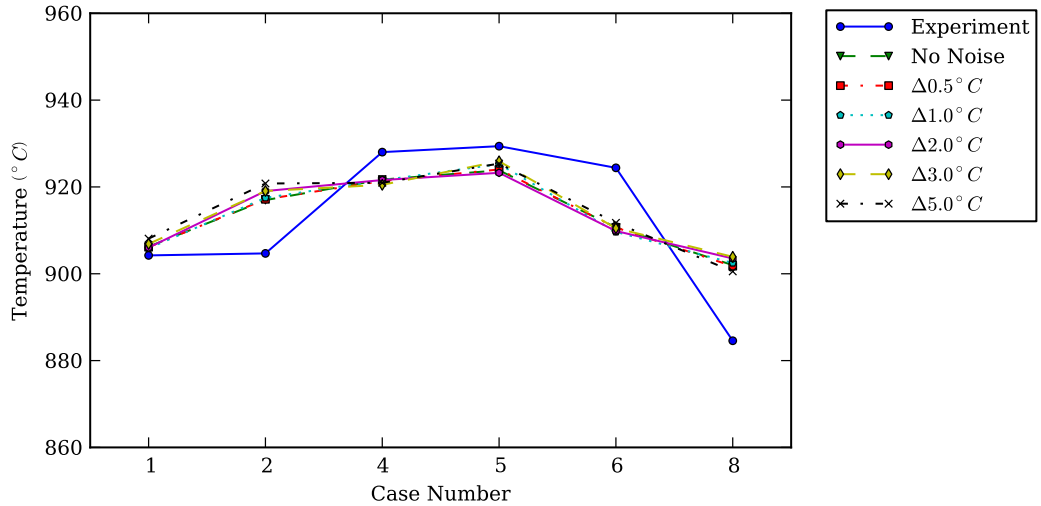

Figure 3.1: Data from the forward simulation and estimated surface temperatures from the proposed algorithm including Gaussian noise up levels of a standard deviation of $5°C$. Data was taken from a sensor embedded at 1 mm depth.

6: **end while**
7: Extract peak surface temperature T_p from last CVFEM simulation

3.2 Temperature estimation results

The algorithm proposed in §3.1 is now tested with the simulation cases used in the sensitivity study of §2.3. For each case, multiple data sets were created by applying different levels of Gaussian noise to the signal. The procedure described in §3.1 is applied to each data set for every case. Because the experimental data comes from the three-dimensional simulations, the actual surface temperatures are known. This allows a comparison of how well the developed algorithm estimated the maximum surface temperature. Some of the cases in the sensitivity study were redundant, in that they have the same shape or characteristic as another case and have been omitted from the results.

The estimated surface temperatures from the algorithm for the varying degrees of Gaussian noise are presented alongside the data in Figure 3.1. One of the major things to note from these results is that the algorithm is relatively insensitive to noise. The estimations for all noise levels, including that of no noise added, are contained within a narrow band of temperatures for a given case. All cases were run using the value for χ that corresponded with that of the baseline case.

For the first, baseline, case, the algorithm predicted a maximum temperature that is within $4°C$ of the data. For the remainder of the cases, the algorithm either over- or under-predicted the data. These errors can be attributed to the constant value of χ that was used

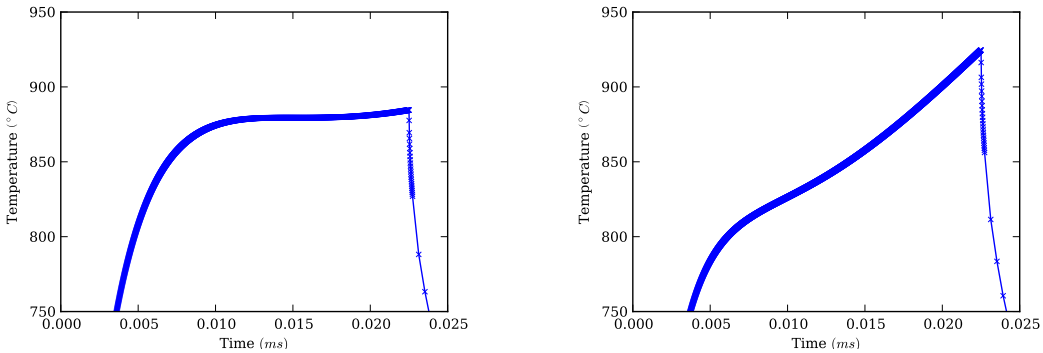

(a) Lower bound.

(b) Upper bound.

Figure 3.2: Temperature profiles representing the bounding conditions.

in all cases, which lead to a nearly constant spread δ. However, Table 2.1 shows that the spread in cases 2-9 are not equal to the spread in case 1, for which χ was developed. Without knowing δ apriori, it will be difficult to exactly predict the surface temperature. However, this correlation of over- and under-predictions leads to an idea of how to estimate a range where the actual data would lie within.

The value of χ used to produce the previous results was chosen to match the value that corresponded with the baseline case. However, the actual value of χ which matches the experimental data will not be known. Reasonable estimates for its bounds are given by two cases. First, the lower bound is given by the case where there is no additional temperature rise after T_s as shown in Figure 3.2a. Second, there is some finite, bounded addition of heat after the initial temperature rise. In this study, it was assumed that the maximum temperature difference from peak to peak was $120°C$. Figure 3.2b shows the upper bound with the $120°C$ temperature rise. The lower bound used is $\chi = 0.250$ and the upper bound used is $\chi = 0.320$, and were chosen with physical understanding of the process.

Each of the cases in Figure 3.1 were re-run using the values of χ corresponding to the lower and upper bounds in order to create a confidence interval for the surface temperature estimation algorithm, and the results of these simulations are shown in Figure 3.3. Only the results for the maximum value of signal noise, $5.0°C$, are presented. These results show that these estimates for the lower and upper bounds of χ create simulations that successfully bound the data from all of the cases run. These data suggest that if the lower and upper bounds of Figure 3.2 are reasonable, then the algorithm can be used to estimate the peak surface temperature $\pm \sim 20°C$.

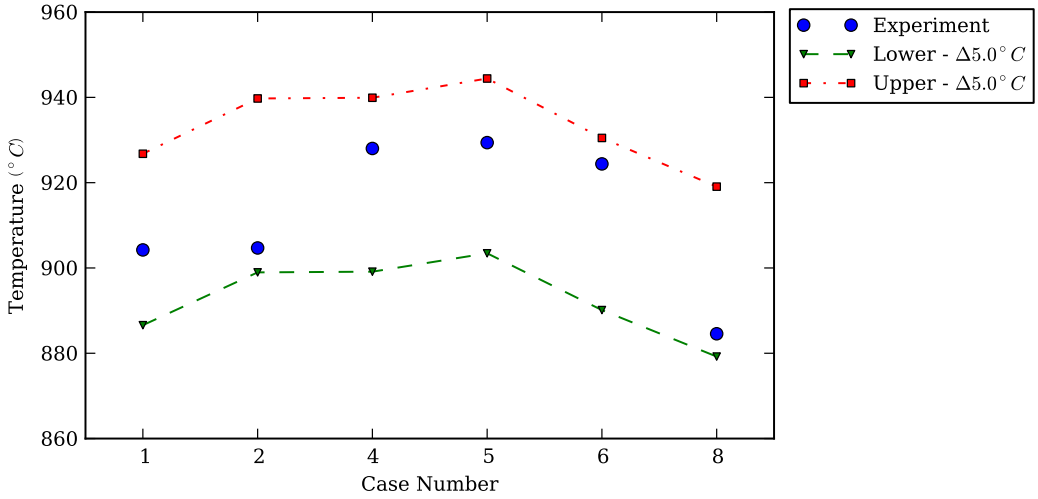

Figure 3.3: Estimated bounds on surface temperatures for a sensor depth of 1 mm with Gaussian noise of $5°C$.

Chapter 4

Conclusions

In this report we have investigated two algorithms for estimating the surface temperature history of a copper bar that has been subjected to a unique, transient, high-energy surface deposition process. A temperature sensor embedded within the bar will be used to gather internal temperature histories, which will then be regressed to estimate the surface temperature.

The initial, naïve approach is to directly correlate the maximum sensor temperature with the peak surface temperature. Due to the rate of deposition and the highly diffusive nature of copper, transient temperatures underneath the surface are both delayed in time and greatly attenuated in magnitude. Thus, correlating the maximum temperature from an embedded sensor to the peak surface temperature is not viable. The sensor would have to be accurate to less than $1°C$ to obtain surface data $\pm 20°C$. If noise is present in the sensor signal, even a highly accurate sensor would lead to spurious estimations.

The second approach is an algorithm which involves fitting the solution to a one-dimensional instantaneous energy solution problem to both the sensor data and to the results of a one-dimensional CVFEM code. This algorithm was shown to be insensitive to Gaussian noise. If the shape of the energy deposition profile is known, then the surface temperature can be predicted very accurately ($\sim 2°C$). For reasonable bounds on the acceptable values of the shape of the energy deposition function, we have shown that the maximum surface temperature can be estimated to within $\pm \sim 20°C$ for all of the cases that were tested.

The analytical model and CVFEM code both assume the probe point is responding to the heat flux applied at a point directly above it on the surface. In reality (and in the forward model) the probe point is responding to all points on the surface applied at all times. There is information convolved in the time-temperature trace in Figure 2.4b that could be extracted with a better analytical model. One candidate would be the canonical case of a rectangular patch heat source propagating over the surface of a semi-infinite wall [3, Section 10.7, Case IX].

Work still needs to be done to experimentally prove this technique. The proposed instrumentation for the embedded sensor is a infrared (IR) detector coupled with fiber optics. The IR detector provides the required sensitivity and speed necessary to record the experimental data. The fiber optic cable can be inserted in a hole drilled from the bottom of the bar. Another important benefit from using IR fiber optics to sense the temperatures is

that it is of low thermal mass. A smaller scale experiment using a lower power laser heat source can be done to calibrate and verify the sensor and proposed temperature estimation technique. After the successful demonstration of this experiment, the instrumentation can then be applied to the full physical system.

References

[1] J. V. Beck, B. Blackwell, and C. R. St. Clair Jr. *Inverse Heat Conduction: Ill-Posed Problems*. John Wiley and Sons Inc., 1985.

[2] T. D. Blacker, W. J. Bohnhoff, and T. L Edwards. CUBIT mesh generation environment. Volume 1: Users manual. Technical report, SAND–94-1100, Sandia National Laboratories, 1994.

[3] H. S. Carslaw and J. C. Jaeger. *Conduction of heat in solids*. Clarendon Press, 1959.

[4] S. Kohli, C. Guo, and S. Malkin. Energy partition to the workpiece for grinding with aluminum oxide and CBN abrasive wheels. *Journal of Engineering for Industry*, 117(2):160–168, May 1995.

[5] S. G. Lambrakos and J. G. Michopoulos. On a general parameterization for inverse analysis of heat deposition processes. *Journal of Materials Engineering and Performance*, 17:411–421, 2008.

[6] S. G. Lambrakos and J. G. Michopoulos. Inverse analysis of rapid and localized energy deposition. *Journal of Materials Engineering and Performance*, 19:928–935, 2010.

[7] S. G. Lambrakos, J. G. Michopoulos, H. N. Jones, and C. N. Boyer. Inverse analysis of heat conduction in hollow cylinders with asymmetric source distributions. *Journal of Materials Engineering and Performance*, 17:651–661, 2008.

[8] A. F. Mills. *Heat Transfer*. Prentice Hall, Inc., second edition, 1999.

[9] A. Y. C. Nee and A. O. Tay. On the measurement of surface grinding temperature. *International Journal of Machine Tool Design and Research*, 21(34):279 – 291, 1981.

[10] P. K. Notz, S. R. Subia, M. M. Hopkins, H. K. Moffat, and D. R. Noble. ARIA manual Aria 1.5: User's manual. Technical Report SAND2007-2734, Sandia National Laboratories, 2007.

[11] Y. Rabin and D. Rittel. A model for the time response of solid-embedded thermocouples. *Experimental Mechanics*, 39(2):132–136, 1999.

[12] D. Rittel. Transient temperature measurement using embedded thermocouples. *Experimental Mechanics*, 38(2):73–78, 1998.

[13] T. Ueda, K. Yamada, and T. Sugita. Measurement of grinding temperature of ceramics using infrared radiation pyrometer with optical fiber. *Journal of Engineering for Industry*, 114(3):317–322, August 1992.

[14] X. Xu. Experimental study on temperatures and energy partition at the diamondgranite interface in grinding. *Tribology International*, 34(6):419 – 426, 2001.

[15] B. Zhu. *Thermal aspects of ceramic grinding*. PhD thesis, University of Massachusetts, 1996.

DISTRIBUTION:

1 David Drewry
Applied Physics Laboratory, Johns Hopkins University
David.Drewry@jhuapl.edu (electronic copy)

1 Bohdan Cybyk
Applied Physics Laboratory, Johns Hopkins University
Bohdan.Cybyk@jhuapl.edu (electronic copy)

1 Keith Lewis
Naval Surface Warfare Center, Dahlgren Division
keith.b.lewis@navy.mil (electronic copy)

1 John Michopolous
Naval Research Laboratory
john.michopoulos@nrl.navy.mil (electronic copy)

1 Scott Douglass
Naval Research Laboratory
scott.douglass@nrl.navy.mil (electronic copy)

1 Roger Ellis
Office of Naval Research
roger.ellis@navy.mil (electronic copy)

1 Ben McGlasson
Office of Naval Research
ben.mcglasson@navy.mil (electronic copy)

1	MS 0346	Ed Piekos, 1513
1	MS 0359	Randy Schunk, 7911
1	MS 0828	Anthony Geller, 1516
1	MS 0836	Scott Roberts, 1513
1	MS 0836	Tyson Watkins, 1516
1	MS 0840	Daniel Rader, 1513
1	MS 1085	Olga Spahn, 1766
1	MS 1135	Walt Gill, 1532
1	MS 1182	Ronald Kaye, 5445
1	MS 0899	Technical Library, 9536 (electronic copy)

Sandia National Laboratories